Supplementary Information for

Double-Decker Design for High Performance Solid Oxide Cells

Sovann Khan[a*], Kwati Leonard[a], Hyo-Young Kim[b], Wilhelm A. Meulenberg[c,d] Motonori Watanabe[a], Miki Inada,[a,b] Hiroshige Matsumoto[a], John Kilner[e], and Tatsumi Ishihara[a,b,f*]

[a]International Institute for Carbon-Neutral Energy Research, (WPI-I^{2}CNER), Kyushu University, 744 Motooka, Nishi-ku, Fukuoka 819-0395, Japan

[b]Department of Applied Chemistry Faculty of Engineering, Kyushu University 744 Motooka, Nishi-ku, Fukuoka, 819-0395 Japan

[c]Forschungszentrum Jülich GmbH, Institute of Energy Materials and Devices (IMD), Jülich, 52425, Germany

[d]University of Twente, Faculty of Science and Technology, Inorganic Membranes, P. O. Box 217, Enschede, 7500 AE, The Netherlands

[e]Department of Materials, Imperial College London, London SW7 2AZ, U.K.

[f]Department of Automotive Science Graduate School of Integrated Frontier Sciences, Kyushu University 744 Motooka, Nishi-ku, Fukuoka, 819-0395 Japan

*Corresponding authors: khan.sovann.455@m.kyushu-u.ac.jp (S. Khan); ishihara@cstf.kyushu-u.ac.jp (T. Ishihara)

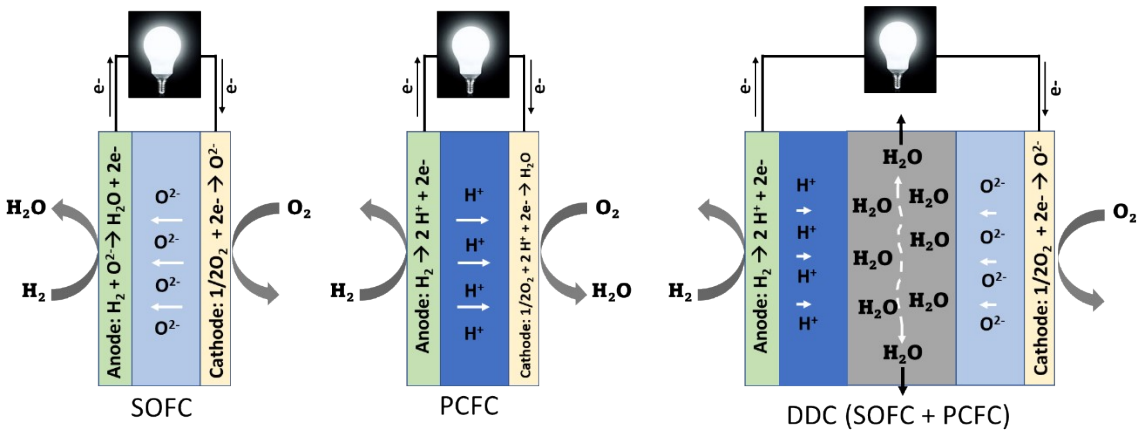

Fig. S1: (a) Concept of dual membrane cell or double decker cell (DDC) by combining oxide-conducting fuel cell or solid oxide fuel cell (SOFC) and proton-conducting fuel cell (PCFC) proposed by previous works [1-5]

Experimental

Materials design of interlayer

The Interlayer is very crucial for making stable and active DDCs. Therefore, careful consideration on material selection was the starting task. The interlayer materials were selected from several criteria as below:

(a) Compatibility:

The delamination due to different materials and compositions would be first examined. The facile way is to include the electrolyte materials. $BaZr_{0.44}Ce_{0.36}Y_{0.2}O_{3-\delta}$ (BZCY) is an electrolyte of PCFC in this work. Therefore, we always included BZCY particles in the interlayer such as NiO-BZCY, $Ce_{0.6}Mn_{0.3}Fe_{0.1}O_{2-\delta}$ (CMF)-BZCY, $La_{0.6}Sr_{0.4}Fe_{0.8}Mn_{0.2}O_{3-\delta}$ (LSFM)-BZCY and LSGM-BZCY) to provide better contact between interlayer and PCFC.

(b) Catalytic ability:

The interlayer should be an active air electrode for PCFCs and fuel electrode for SOFCs. Therefore, we selected materials which were commonly used such as NiO, CMF, LSFM, and LSCF including in the interlayer materials. Typically, CMF and LSFM can be used for both fuel and air electrode materials [6-8]. Although there are more materials available, we could not test all materials in this report.

(c) Conductivities:

Interlayer materials should possess high ionic and electronic conducting. In this case, we consider oxide conducting materials (e.g., LSGM [9]), proton conducting materials (BZCY, BZCYYb , LSS [10, 11]) and mixed ionic and electronic conducting materials (LSFM, CMF [6-8])

Based on these criteria, materials were selected for interlayer electrode which were expected to be active for DDC fabrication.

Material synthesis

$BaZr_{0.44}Ce_{0.36}Y_{0.2}O_{3-\delta}$ (BZCY), $BaZr_{0.16}Ce_{0.64}Y_{0.1}Yb_{0.1}O_{3-\delta}$ (BZCYYb) and **$SrZr_{0.5}Ce_{0.4}Y_{0.1}O_{3-\delta}$ (SZCY)** were purchased from domestic manufacturers (KUSAKA RARE METAL PRODUCTS CO., LTD, Japan).

$La_{0.6}Sr_{0.4}Co_{0.2}Fe_{0.8}O_{3-\delta}$ (LSCF), $La_{0.6}Sr_{0.4}Fe_{0.8}Mn_{0.2}O_{3-\delta}$ (SLFM), $La_{0.85}Sr_{0.15}ScO_{3-\delta}$ (LSS), $Ce_{0.6}Mn_{0.3}Fe_{0.1}O_{2-\delta}$ (CMF), $Ba_{0.6}La_{0.4}CoO_{3-\delta}$ (BLC) powder were prepared by the pechini process (with citric acid) using nitrate solution. The calculated metal nitrates were dissolved in 200 mL of distilled water. Then, EDTA and citric acid as chelating reagent were added and stirred to evaporate water at 290 ℃ with glass cover which was suppress incomplete reaction from rapid evaporation rate. At this stage, gel formation was observed by results of metal complexation and with gelation was completed, magnetic bar was removed and heated at 400 ℃ until become the black powder. The obtained powder was pre-calcined at 400 ℃ for 2h. The final annealing was conducted at temperature range from 900~1200 ^{o}C for 6 h.

$La_{0.9}Sr_{0.1}Ga_{0.8}Mg_{0.2}O_{3-\delta}$ (LSGM) was synthesized by solid-state reaction. With stoichiometric ratio of LSGM, 9.79 g of power composed of La_2O_3 (99.99%, Kishida, Japan), $Sr(CO_3)$ (99.99%, Wako Pure Chemical Industries Co., Ltd, Japan), Ga_2O_3 (99.99%. Wako Pure Chemical Industries Co., Ltd, Japan), MgO (99.9%, Wako Pure Chemical Industries Co., Ltd, Japan) were mixed with ethanol by planetary ball-milling (20 zirconia balls, 5-mm diameter) for 12 h (48 cycles of 15-min run and 5-min rest). Then, LSGM powder was annealed at 1000 ^{o}C for 6 h in air.

Electrochemical performance: Two sets of home-made alumina tubes were used for air chamber and fuel chamber (Fig. S2(b)). Each set is composed of two different sizes of alumina tubes and connected to each other by different sizes of Swagelok systems. The tip of the inner tube is covered by Pt-mesh current collector contacted to another Pt mess covering the electrode for current collector. **At air chamber**, inlet gases (O_2/Air/Steam) are supplied through the outer alumina tube into the cell and flow out through the inner alumina tube. Both feed and formed O_2 flow though the outlet toward the waste line. **At fuel chamber**, fuel gases (H_2/N_2) are supplied through inner alumina tube and flow outward through outer alumina tube. Both feed and formed H_2 flow through the outlet toward the waste line. H_2 quantification was conducted from the outlet gas downstream of fuel outlet.

Cell is placed between two sets of alumina tubes and sealed by glass-sealing. This cell analysis system was placed into tubular furnace for controlling the reaction temperature.

Table S1: Gas compositions used for electrochemical analysis

	Support reduction	**FC**	**EC**
Fuel electrode (bottom)	humid H_2	humid H_2	humid 10%H_2-90%N_2
Air electrode (Top)	humid O_2	humid O_2	50%O_2-50%steam

After setting up the cell, the temperature increased to 800 ^oC (3.3 ^oC min^{-1}) and kept for 1 hour for glass-sealing. Before electrochemical measurement, fuel support (NiO-SZCY) was reduced by humid hydrogen at 700 ^oC for more than 1 hour. During FC analysis, 100 mL/min of H_2 (humid) is supplied into support side, and 100 mL/min of O_2 (humid) is supplied into air electrode site (BLC). After FC operation, reaction is shifted to EC operation with gas composition of 10 mL/min H_2 (10%)-90 mL/min N_2 (90%) (fuel electrode side) and 50 mL/min O_2-0.04 mL/min of water (air electrode). For generating steam, a constant flowrate of water (0.04 mL/min) was pumped into high-temperature evaporator and carried by 50 mL/min of O_2 at the outlet of evaporator to achieve the gas composition of 50 mol% O_2 and 50 mol% H_2O at the inlet of reactor into the air electrode chamber (see Table S1). Electrochemical analysis of cells such as current-voltage-power (I-V-P) measurement is conducted from reaction temperature of 500 ^oC by using four-wire method, called separate current and voltage leads. The current across the cell is controlled by using a Potentiostat/Galvanostat (HAL3001, Hokuto Denko, Japan), and terminal voltage is measured by a digital multimeter (R6451A, Advantest, Japan). overpotential and internal resistance (IR) is analyzed by current interruption method [12]. A constant current-pulse is generated by a current pulse generator (HC-111, Hokuto Denko, Japan), and transient potential responses are monitored with a memory hicorder (8835, Hoiko, Japan). Electrical impedance spectra (EIS) of electrodes are measured with an impedance/gain-phase analyzer (SI 1260 impedance analyzer and SI 1287, Solartron, Farnborough, UK) with commercial Z-view software under open-circuit condition at AC voltage of 10-25 mV and frequency range

of 10^5 to 0.1 Hz.

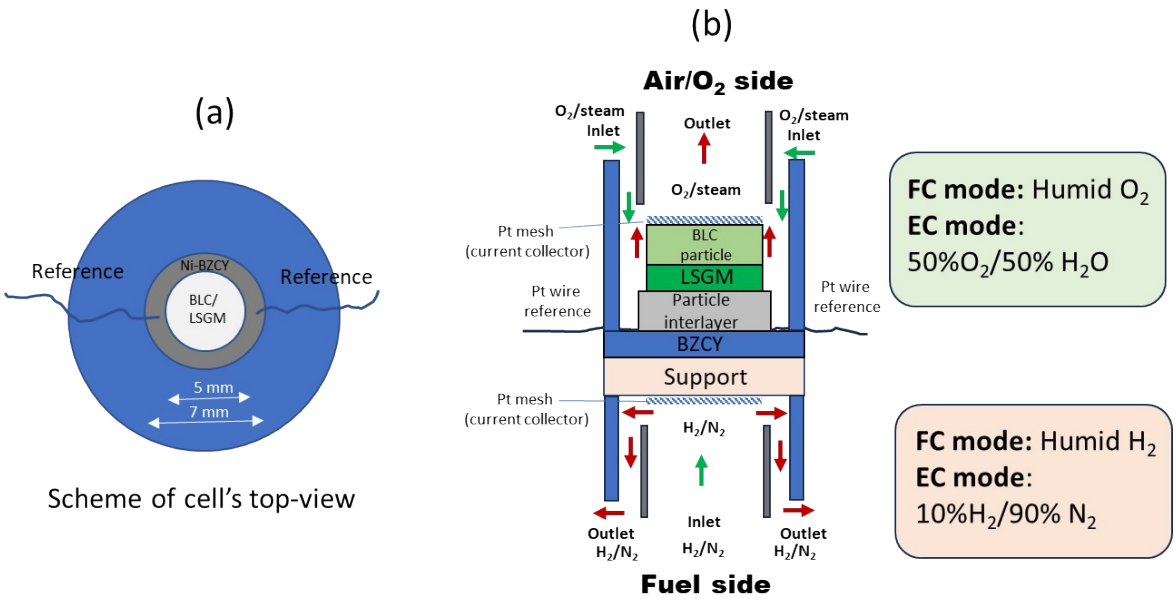

Fig. S2: Cell's structure and reactor configuration

Faradaic efficiency calculations

$$Faradaic\ efficiency\ (\%) = \frac{H_2\ formed}{H_2\ calculated\ by\ Faraday\ law} X\ 100 \qquad (eq.\ S1)$$

H_2 formed was measured by Gas Chromatography equipped with a thermal conductivity detector (GC-TCD) per area of air electrode (0.2 cm^2). While the theoretical H_2 was calculated by Faraday law below:

$$H_2\ calculated\ by\ faraday\ law\ (mol) = \frac{1}{2} n_{e^-} = \frac{Q}{F} = \frac{I\ x\ t}{F} \qquad (eq.\ S2)$$

One electron (n_{e^-}) generates ½ H_2 ($2H^+ + 2e^- \rightarrow H_2$). Q is coulombs charge (C). I is electrical current (A) applied at time, t (s). F is Faraday's constant (96485 C/mol of n_{e^-}).

Finally, the number of calculated H_2 will be divided by area of active electrode of air electrode (0.2 cm^2).

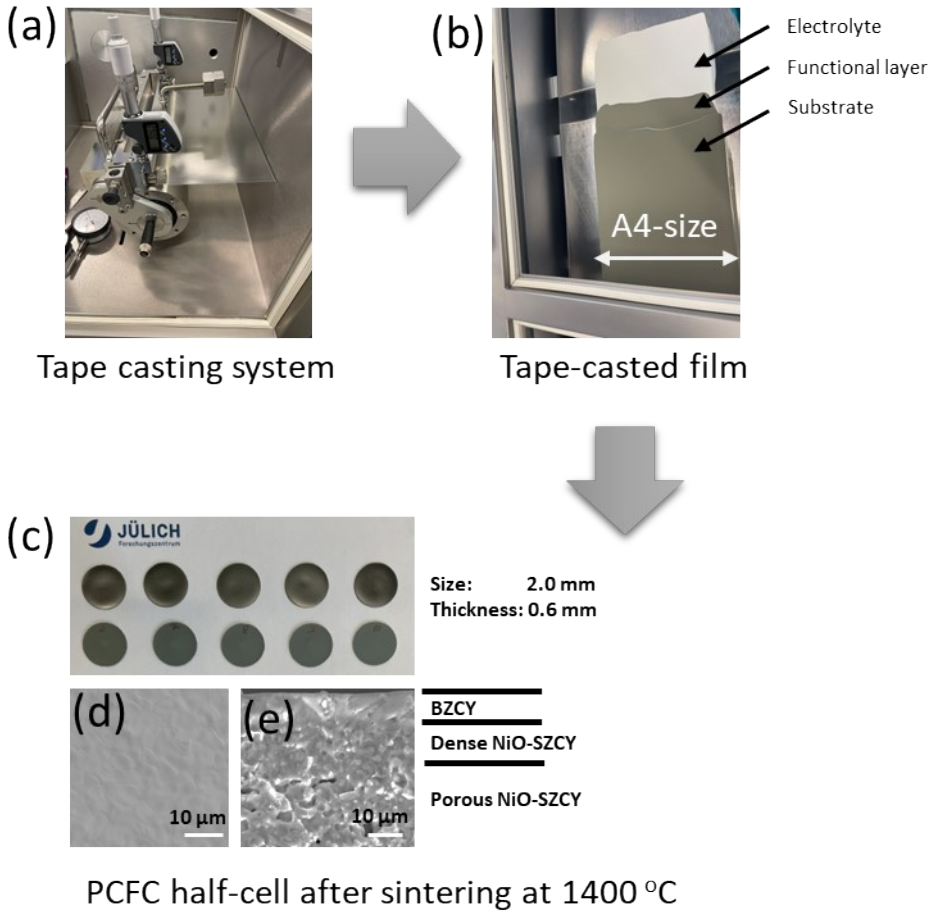

Fig. S3 PCFC preparation process (a) camera image of a Tape-casting system, (b) a Tape-casting film after drying, (c) camera image of cells after sintering at 1400 °C, (d) and (e) SEM images of surface (BZCY) and cross-section of PCFC half-cell

Supplementary Note 1: Protonic ceramic half-cell fabrication and characterizations

Protonic ceramic half-cell was fabricated by Tape-casting method following by co-sintering at 1400 °C for 5 h (Fig. S3. An A4-size green sheet composed of 3 layers (BZCY electrolyte, dense NiO-SZCY functional layer and porous NiO-SZCY substrate). This green

sheet was cut into small cell and sintered to form protonic ceramic half-cell. The electrochemical performance of this half-cell was evaluated by fabricating a single cell by depositing BLC air-electrode on the top of BZCY electrolyte.

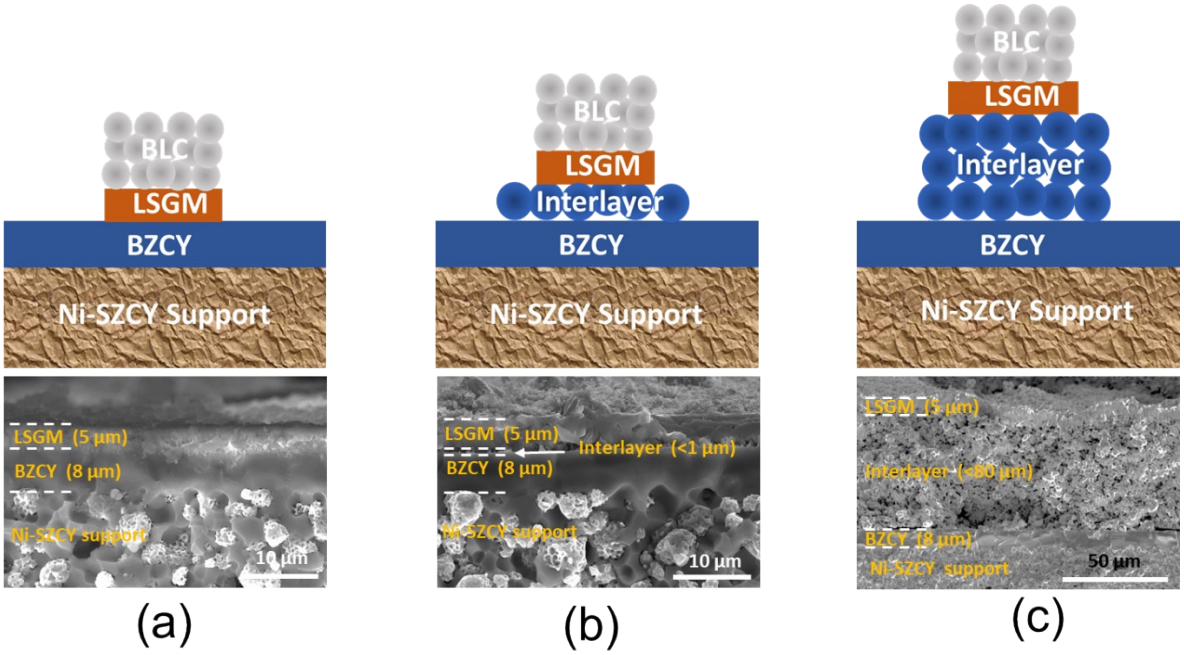

Fig. S4: different types of DDC cells designed based on interlayer: (a) without interlayer, (b) thin interlayer and (c) thick interlayer

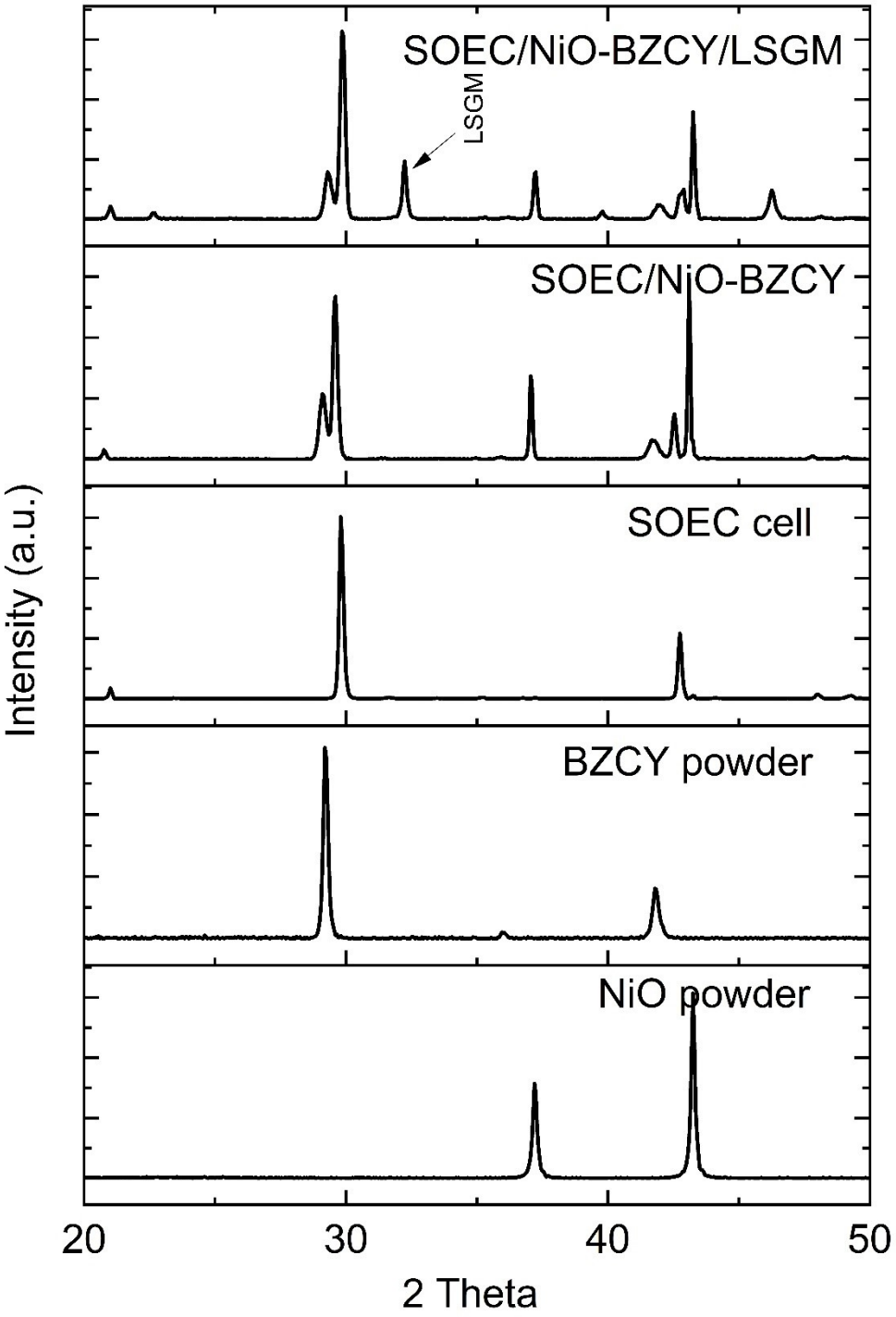

Fig. S5: XRD patterns of each layer deposited.

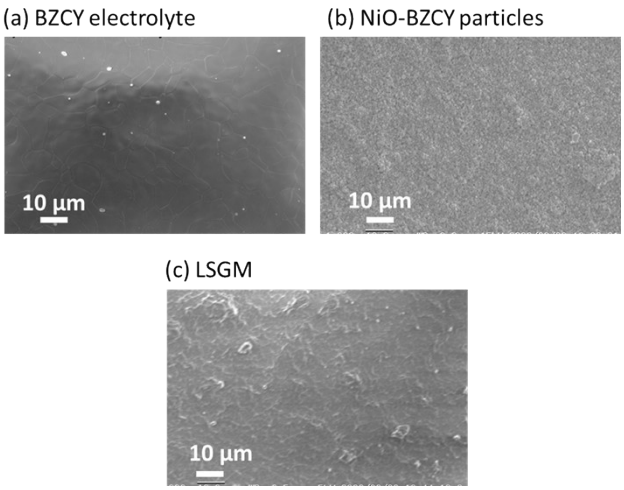

Fig. S6: SEM images of the surface of BZCY electrolyte (a), NiO-BZCY particle interlayer (b) and LSGM film (c), respectively

Supplementary Note 2: Structure of cross-section of DDC

Two cells were selected to represent the difference of interlayer thickness and materials. All images were taken from cells after reaction. Most of the BLC air electrode layer has delaminated after removing the cell from the reactor and was thus not visible on some cells. The selected elements of main compositions were analyzed by EDS mapping to highlight each layer. For example, Ni is representative of the support (NiO-SZCY) and the interlayer (NiO-BZCY particles). La and Ce represent the LSGM and BZCY electrolytes. Fig. S7(a)~(c) shows the cross-section of DDC with a thin NiO-BZCY interlayer. A thick BZCY film (~8 µm) of the main electrolyte with a thinner LSGM secondary electrolyte (~ 5 µm) can be clearly seen. Elemental mapping at two locations from the same cell (location (b) and (c)) with different magnifications allow us to confirm that the very thin interlayer (<1 µm) of NiO-BZCY particles has been successfully deposited between the BZCY and LSGM electrolytes. Another DDC was selected to represent a thicker interlayer composed of only CMF materials. SEM images in Fig. S7(d) show a cross-section of another cell made from a thick interlayer (~30 µm) of CMF particles. Elemental mapping shown in Fig. S7(e), confirms that the CMF particles are well deposited between BZCY and LSGM as an interlayer.

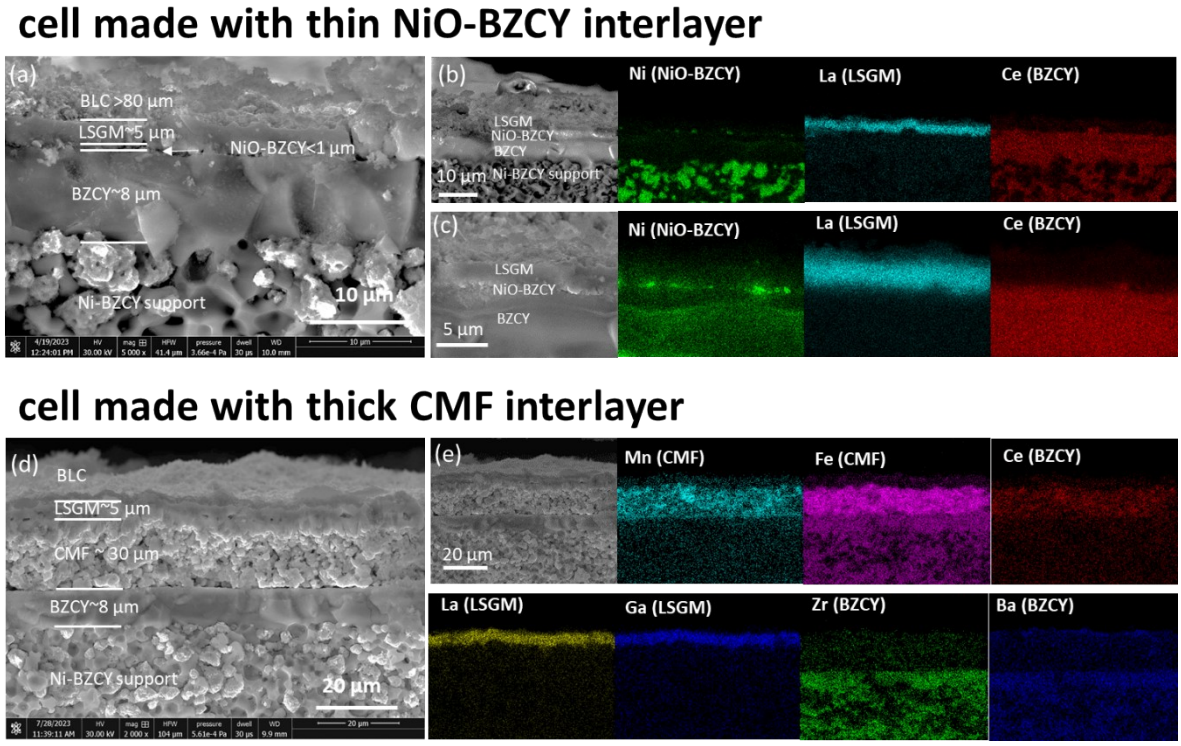

Fig. S7: SEM images of cross-section of the cell after reaction, and elemental mapping of each element: (a)~(c) cell made with a thin NiO-BZCY interlayer, (d)~(e) cell made with a thick CMF interlayer

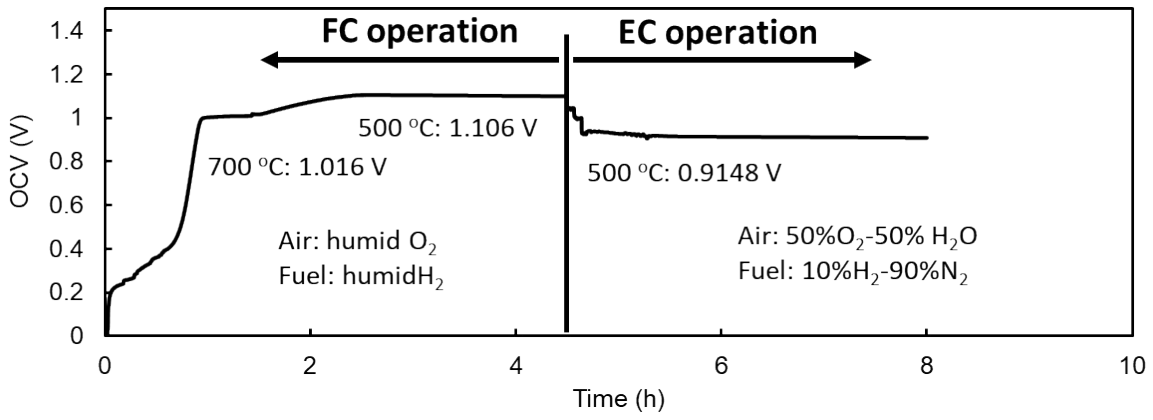

Fig. S8 Open circuit voltage (OCV) of PCFC reference at different gas compositions and temperatures

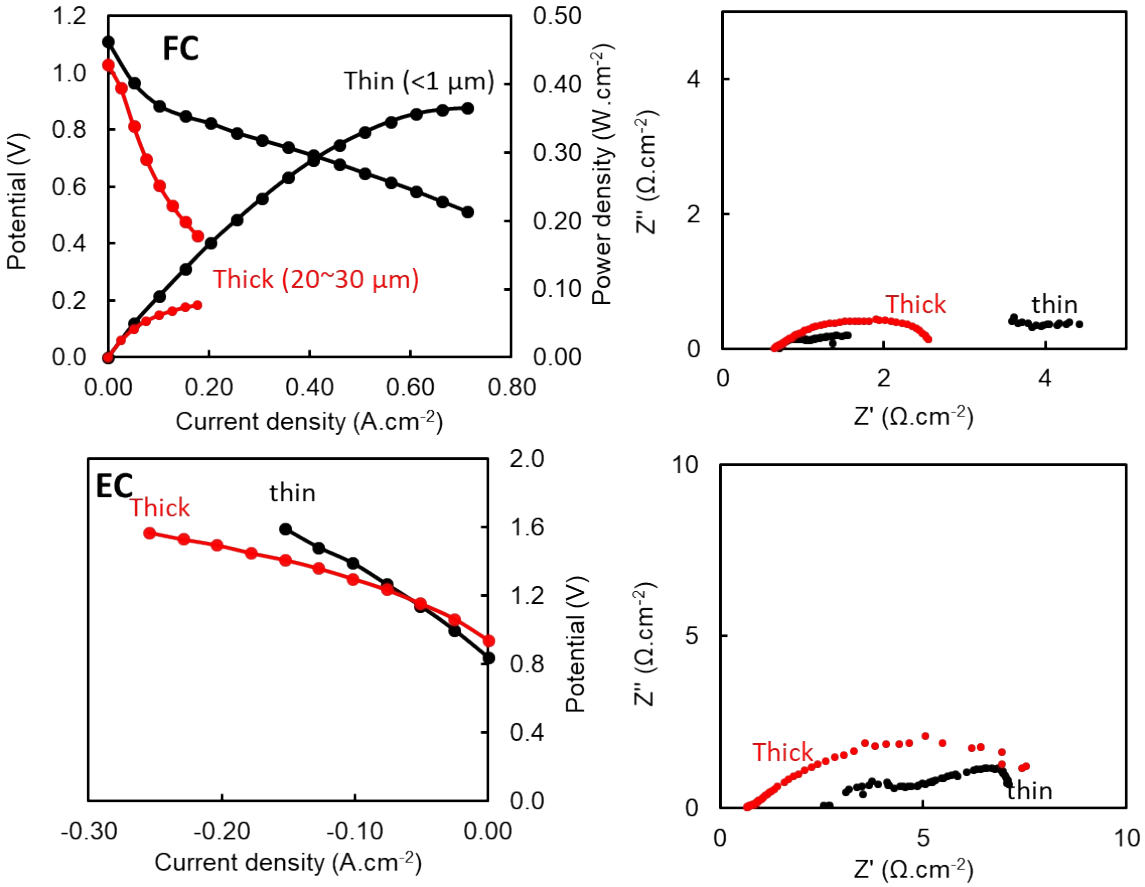

Fig. S9: The effects of interlayer thickness on FC and EC performance of DDC made with CMF-BZCY as interlayer operated at 500 °C

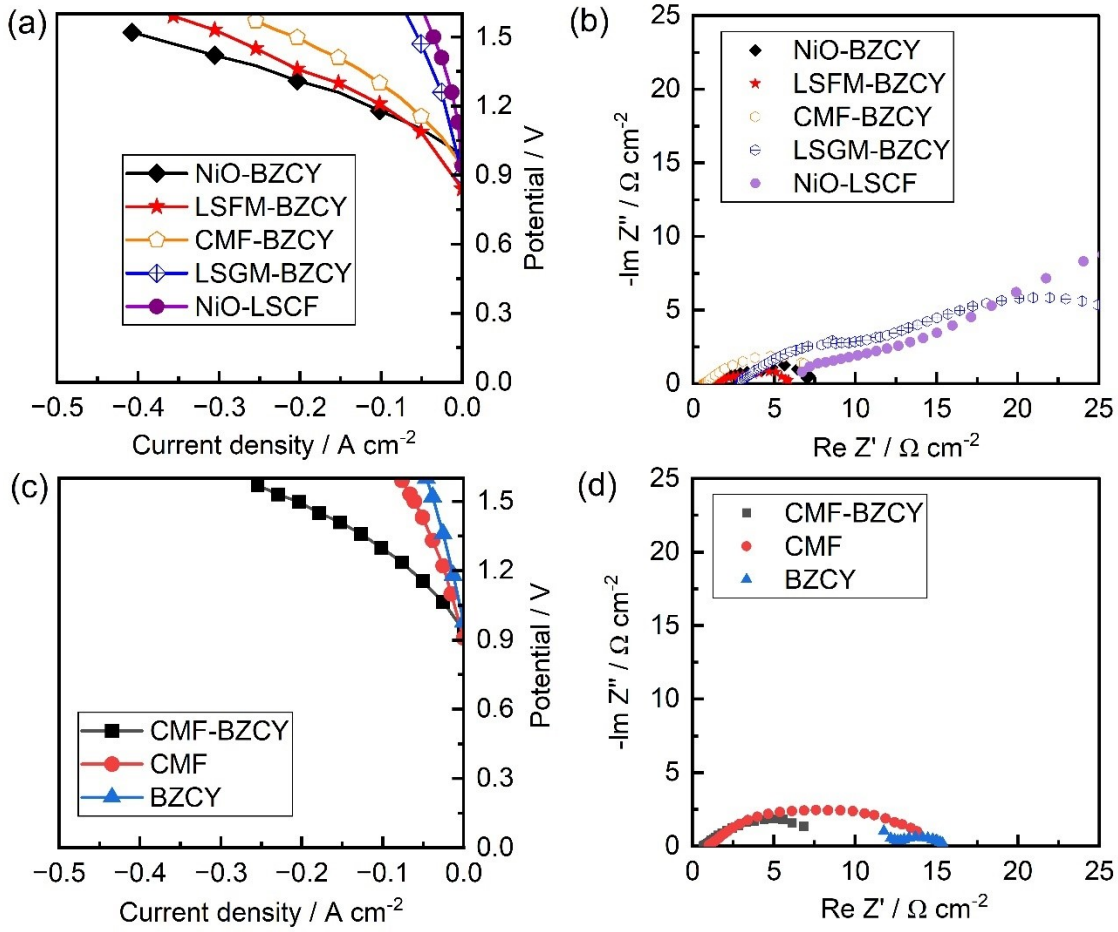

Fig. S10: EC performance at 500 °C of DDCs made with different interlayer-materials: (a) and (b) I-V curves and their corresponding EIS spectra of DDCs made with different composite materials; (c) and (d) I-V and EIS spectra of DDCs made with singe-material interlayer (CMF or BZCY) and composite-material interlayer (6CMF-4BZCY)

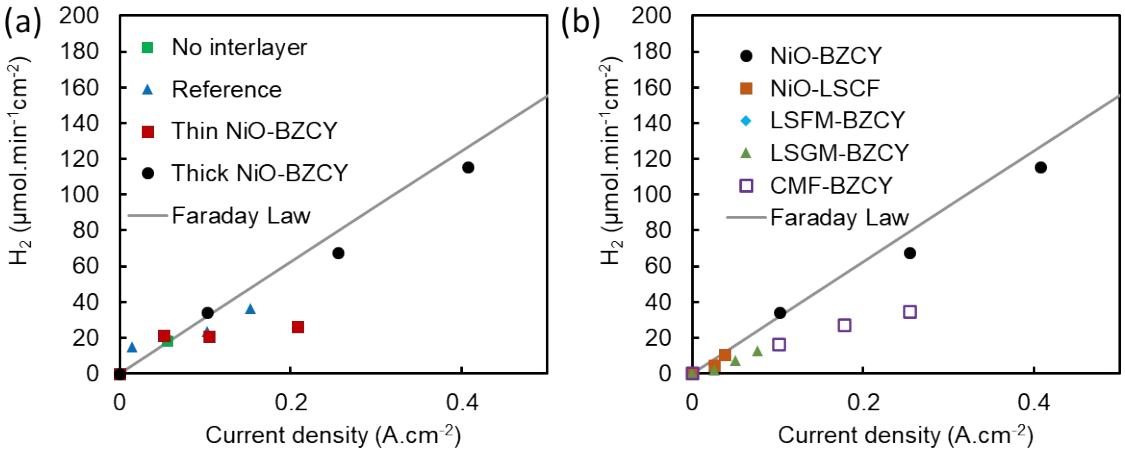

Fig. S11: Hydrogen generation from 500 ºC-EC operation (a) effects of interlayer and thickness and (b) effects of interlayer materials

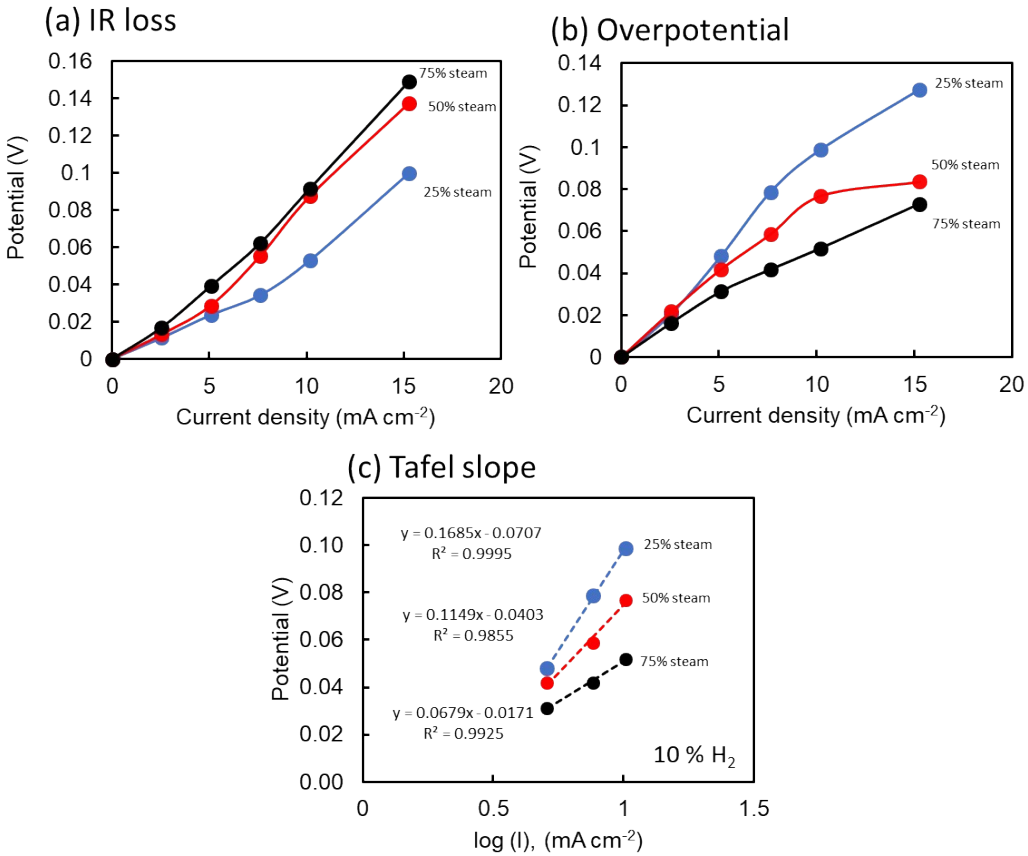

Fig. S12: IR loss, overpotential and Tafel slope of cell made from thick Ni-BZCY interlayer operated at 500 ºC of EC mode

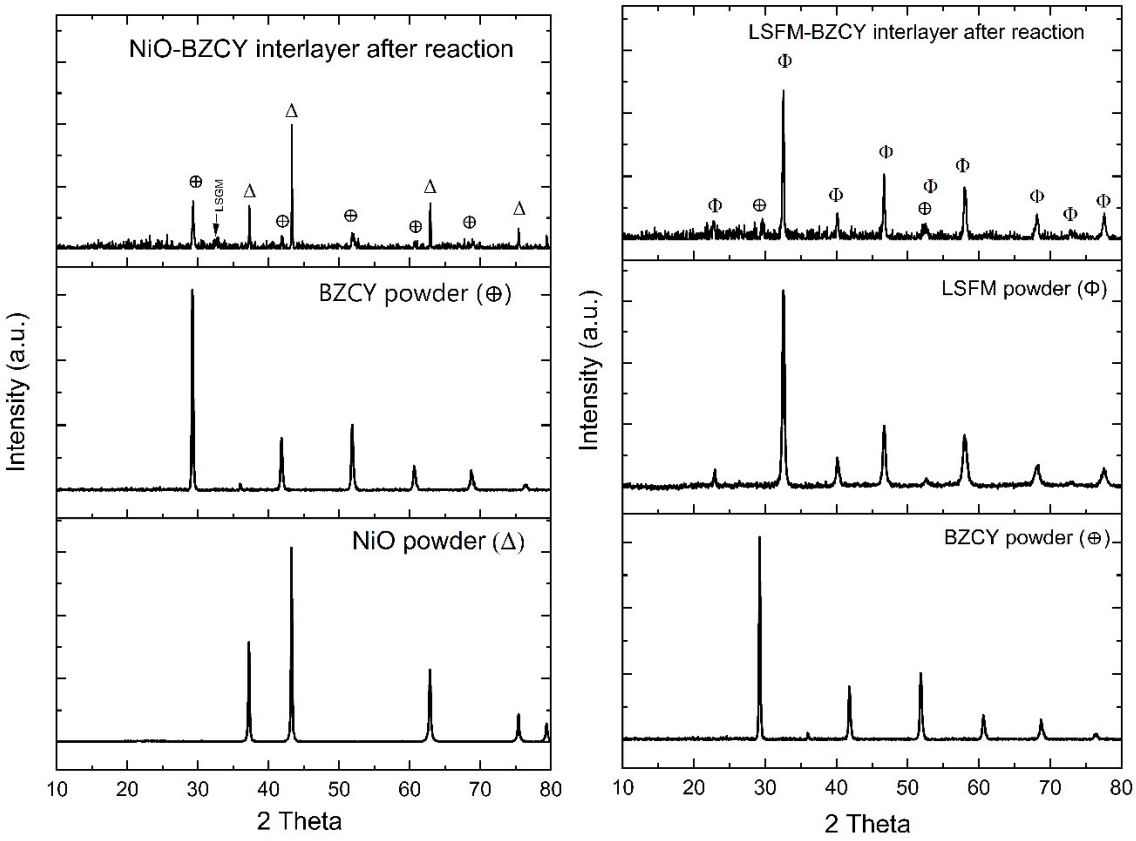

Fig. S13: XRD patterns of interlayer materials (NiO-BZCY and LSFM-BZCY) and their respective single-phase oxides.

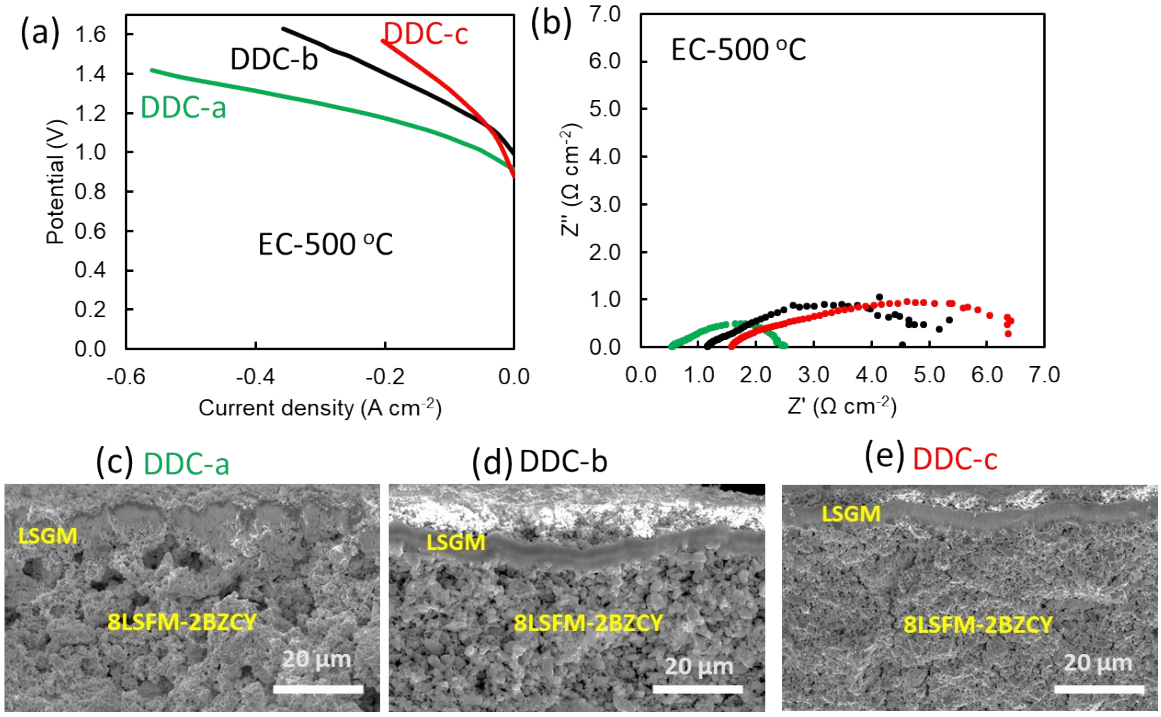

Fig. S14: EC performance at 500 °C of DDCs with different structures of interlayers and their cross-sectional views of cell after reaction: Interlayer materials used without ball-milling (DDC-a), interlayer materials used after 30 min ball-milling (DDC-b) and 2 h ball-milling (DDC-c)

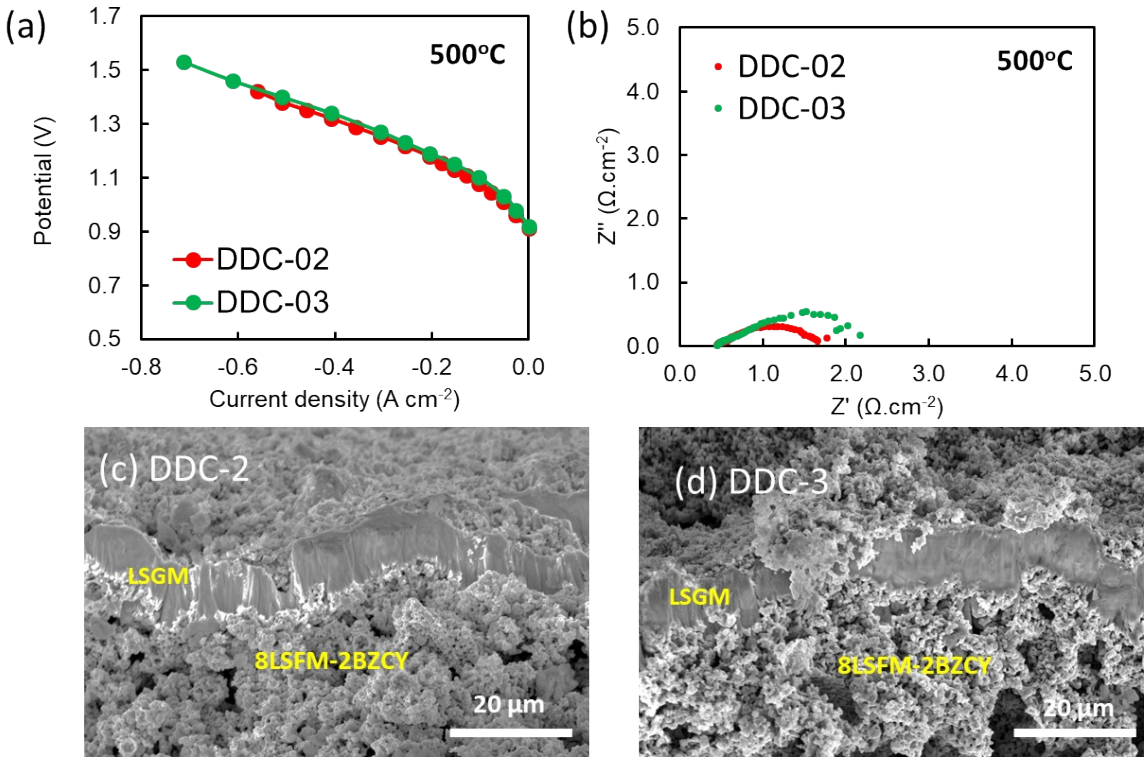

Fig. S15: EC performance at 500 °C of DDCs with the same structures of interlayers and their cross-sectional views of cell after reaction

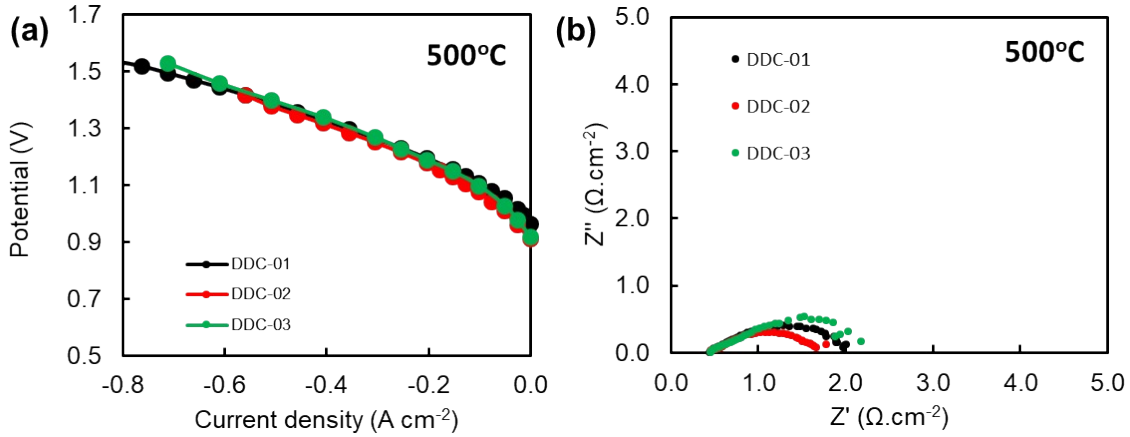

Fig. S16: I-V curves and their corresponding EIS of three DDCs made with 8LFM-2BZCY interlayer operated at 500 °C

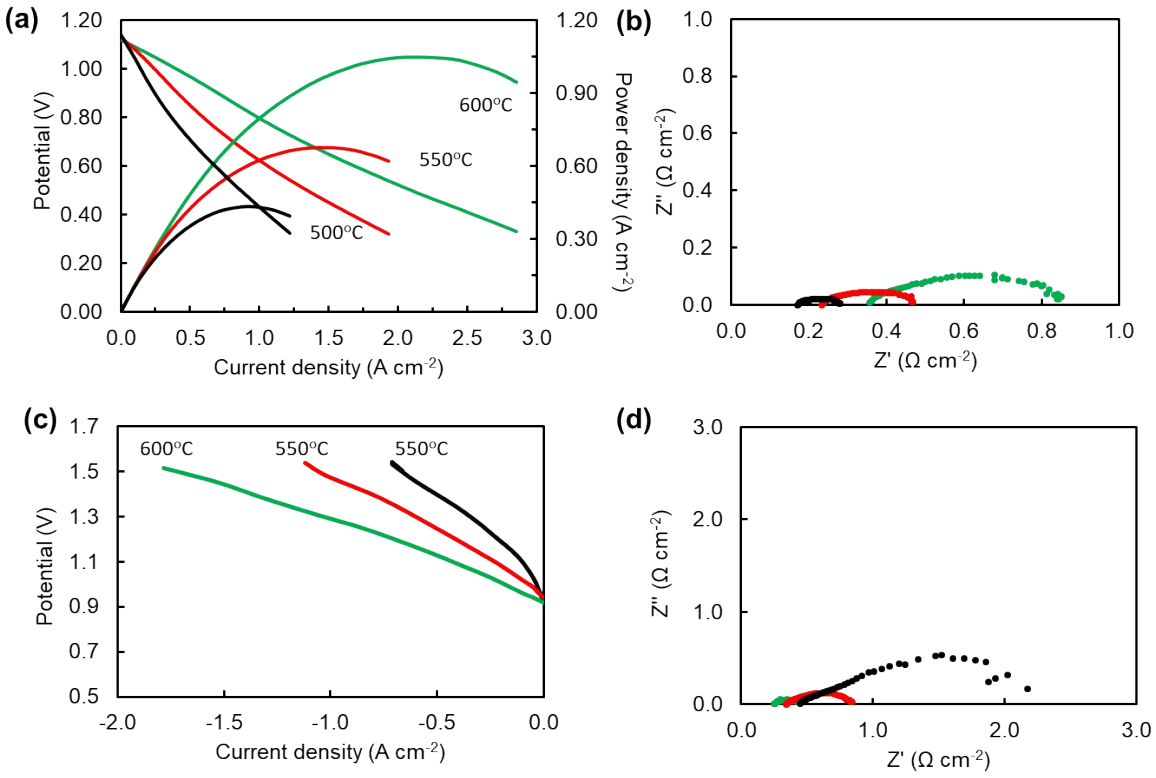

Fig. S17: Electrochemical performance of DDC at different temperatures (a) and (b) I-V, I-P curves and their corresponding EIS spectra of FC operation, (c) and (d) I-V and their corresponding EIS spectra of EC operation. The maximum FC power density was 0.44, 0.68 and 1.05 W cm^{-2} at 500, 550 and 600 °C, respectively. The EC current density at 1.5 V was 0.34, 0.60 and 1.07 A cm^{-2} at 500, 550 and 600 °C, respectively.

Supplementary Note 3: Faradaic efficiency

Due to the p-type electronic leakage across the BZCY electrolyte, Faradaic efficiency is commonly low. In the oxidative atmosphere, hydration, which is a main mechanism for proton transport across the electrolyte via equation (*eq. S3*), is suppressed by oxidation reaction via *eq. S4*.

$$H_2O + V_o^{\bullet\bullet} + O_O^x \leftrightarrow 2OH_O^{\bullet} \quad (eq.\ S3)$$

$$\frac{1}{2}O_2 + V_o^{\bullet\bullet} \rightarrow O_O^x + 2h^{\bullet} \quad (eq.\ S4)$$

The low Faradaic efficiency is one the main challenges in protonic ceramic cells, typically in the high oxygen-partial pressure atmosphere. Therefore, our previous works used low oxygen-partial pressure (e.g., 1% O_2 diluted in inert gas and steam) for steam electrolysis to achieve a reasonable Faradaic efficiency (80~88% at applied voltage 1.3~1.6 V) [11, 13, 14].

By using the same type of protonic ceramic cell as our previous reports, DDC provides better Faradaic efficiency in highly oxidative atmosphere (50% O_2 diluted in inert gas and steam). DDC made with 6LSFM-4BZCY interlayer generated H_2 with 95% Faradaic efficiency at 1.5 V (see Fig. S18(a)). The better current density of DDC with 8LSFM-2BZCY interlayer generated lower Faradaic efficiency of 70~80% at 1.5 V. However, if this cell was operated at 1.3 V, Faradaic efficiency is high ~ 90% (Fig. S18(b)).

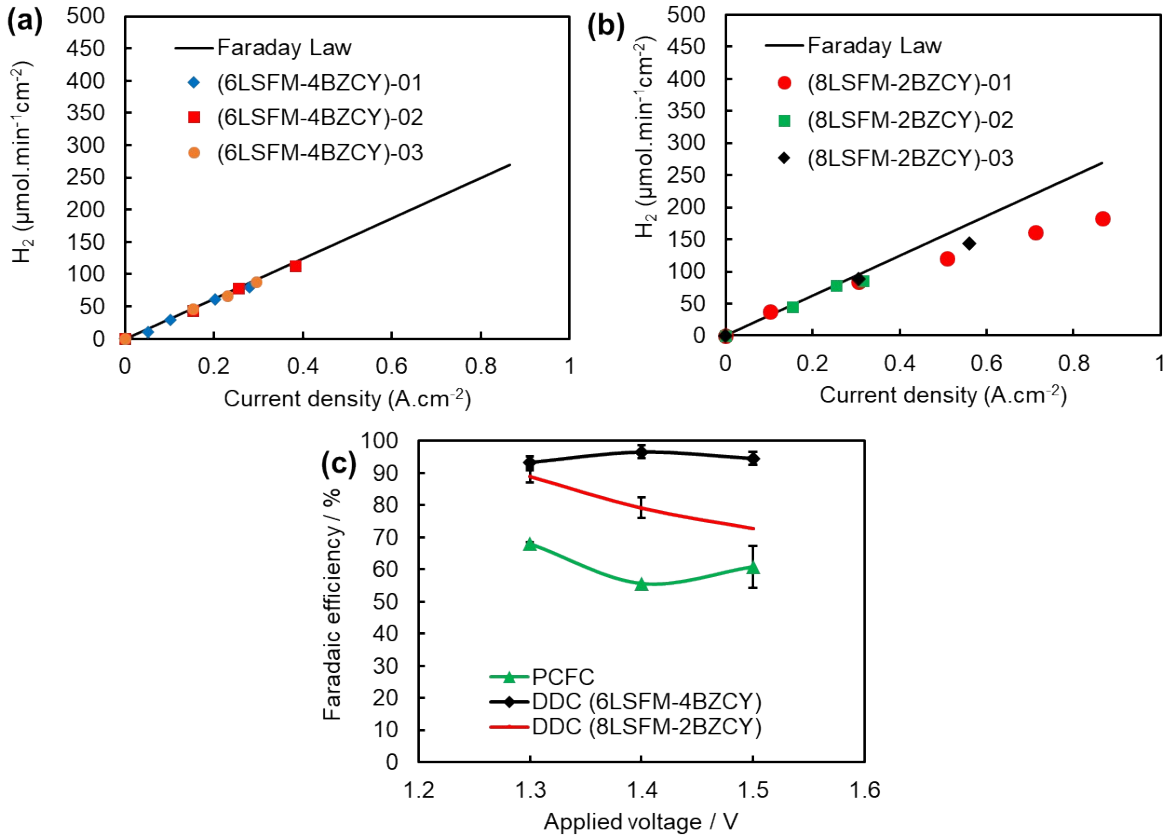

Fig. S18: Summary of hydrogen generation from EC 500°C (a) DDC with 6LSFM-4BZCY interlayer, (b) DDC with 8LSFM-2BZCY interlayer, (c) average Faraday Efficiency [3 cells of each type of cell were selected]

Supplementary Note 4: Long-term operation of DDC

First, a PCFC cell was analyzed its EC for a longer operation. In Fig. S19 showed EC operation at a constant current density of 0.082 A cm^{-2} at 500 °C. The initial voltage was ~1.31 V after more than 40 hours, the voltage increased to 1.35 V. The faradaic efficiency was significantly reduced after 48 hours.

A DDC with 8LSFM-2BZCY as interlayer was selected for long-term EC operation (see Fig. S20). This cell was initially operated at 1.3 V for 140 h, and then, at 1.5 V for the rest of time. The degradation was observed at 48 h. The potential increased by 62 mV after

48 h. After that, only minor degradation was observed. From 48 h to 140 h, the potential was increased by 28 mV. From 140 h to 207 h, the potential increased by 18 mV. More interestingly, the Faraday efficiency was still high (~90%) after 200 h of operation. This confirmed the DDC enables to produce hydrogen from steam electrolysis more efficiently than that of conventional PCFC.

After reaction, cell's cross-section was analyzed by SEM/EDS (see Fig. S21 and S22). After the long-term test, the cell still maintained in good condition with all layers. No significant delamination was observed. This cell is composed of a very thick interlayer (130 µm). This very thick interlayer might be one of the reasons for the low performance of cells. The optimized thickness interlayer was 80~90 µm. However, due to the different surface-flatness of photonic ceramic half-cell, it was hard to deposit the same thickness from cell to cell. In addition, the EDS elemental mapping of main elements confirmed that all layers composted of target materials: NiO-SZCY substrate, BZCY electrolyte, LSFM-BZCY interlayer, LSGM dense film, and BLC air electrode.

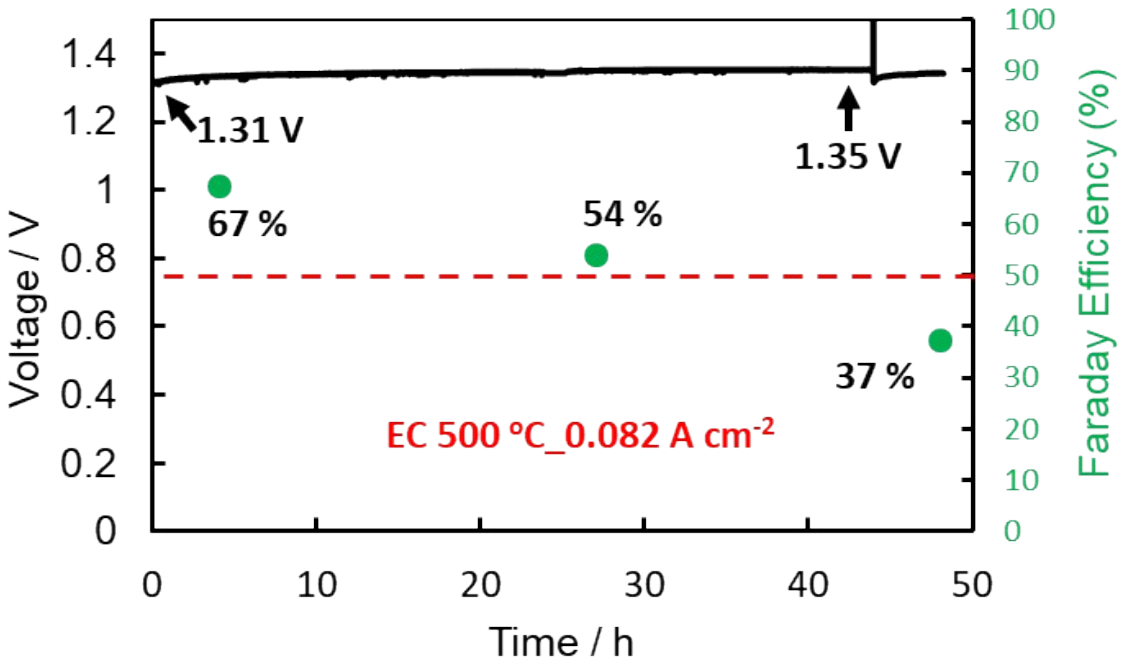

Fig. S19 Steam electrolysis of PCFC reference cell at 500 °C for 48 hours

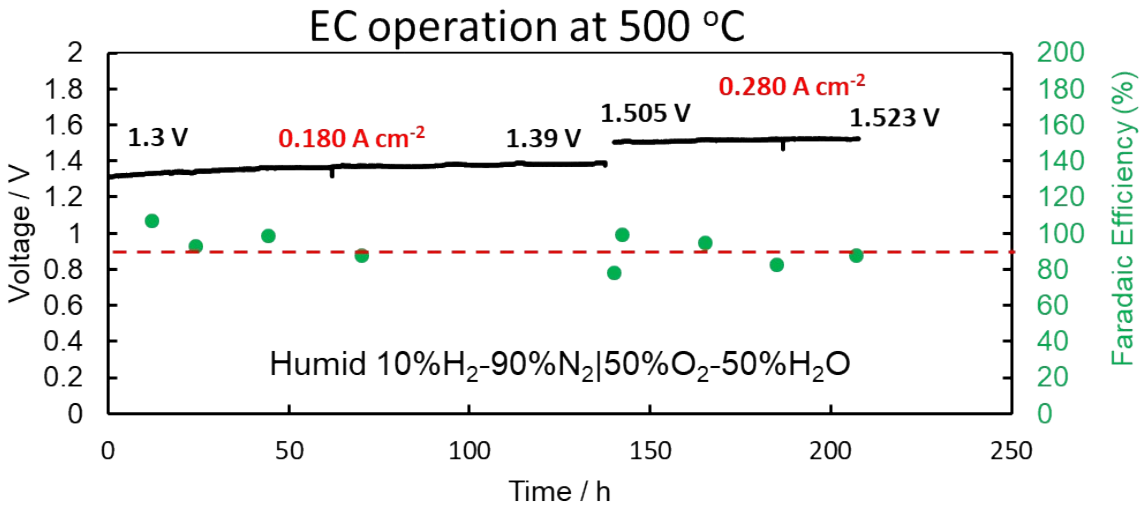

Fig. S20: Long-term operation of DDC made with 8LSFM-2BZCY interlayer at 500 °C

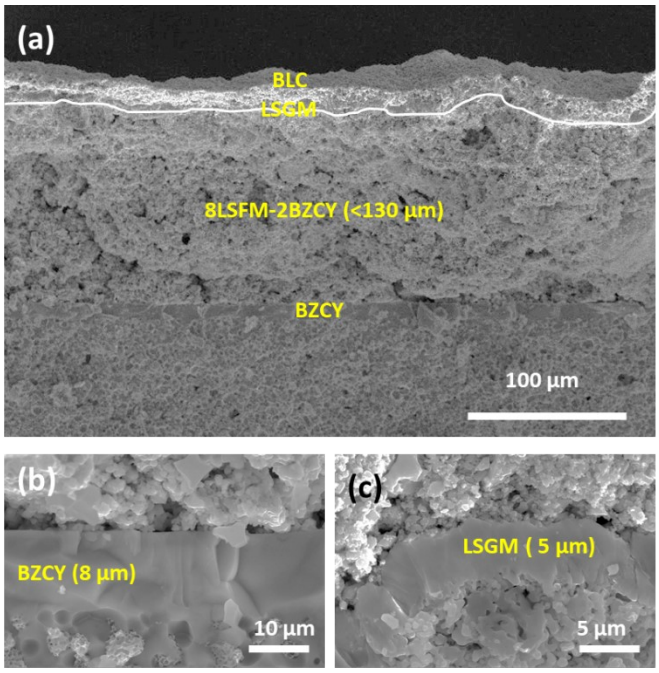

Fig. S21: SEM of cross-section of DDC after 200-hour operation,

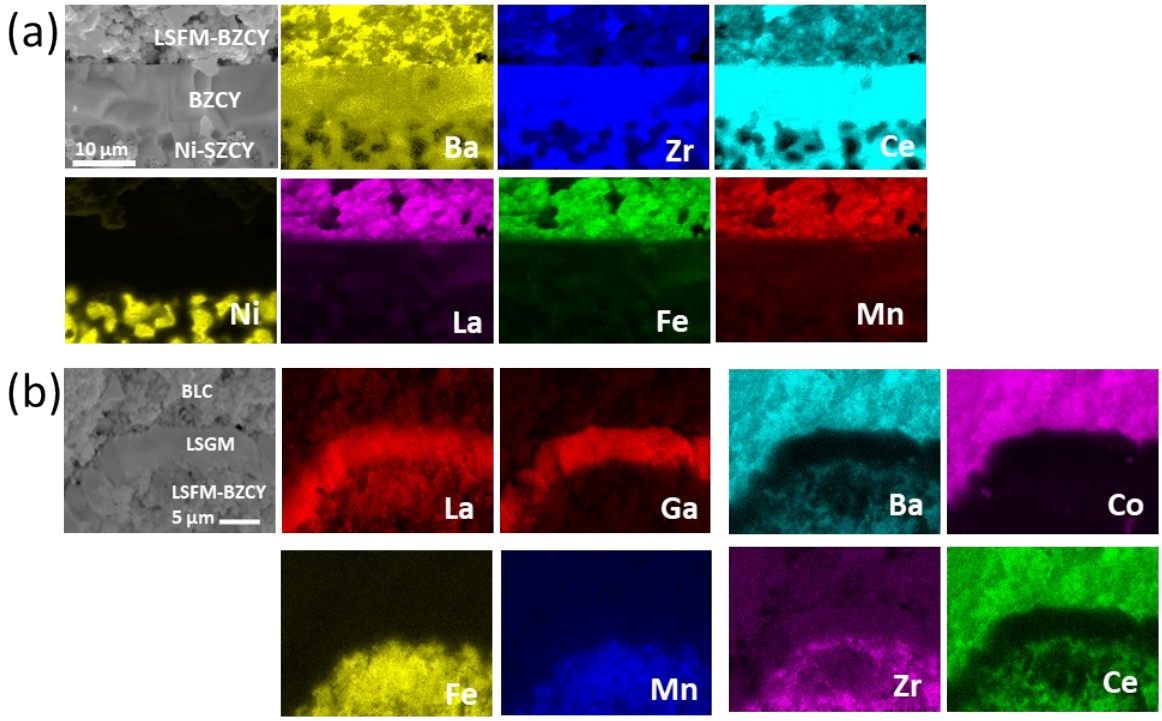

Fig. S22: SEM of cross-section of DDC after 200-hour operation

Table S2: summary of FC cell performance at 500 ^{o}C

Cell/interlayer	**OCV (V)**	**Power Density (W cm^{-2})**	**Polarization Res. (Ω cm^{-2})**	**Ohmic loss (Ω cm^{-2})**
Reference	1.106	0.22	2.05	0.78
No interlayer	1.07	0.16	2.59	1.78
6NiO-4BZCY (<1 μm)	1.09	0.27	1.43	0.63
6NiO-4BZCY (20-30 μm)	1.13	0.08	3.97	0.51
6NiO-4BZCY (60-70 μm)	1.16	0.04	4.8	2.33
6CMF-4BZCY (<1 μm)	1.12	0.37	0.85	0.71
6CMF-4BZCY (20-30 μm)	1.04	0.08	1.91	0.64
6NiO-4LSCF (20-30 μm)	1.13	0.016	37.99	6.06
6LSS-4BZCY (20-30 μm)	1.09	0.02	15.29	0.94
NiO-BZCYYb (20-30 μm)	1.09	0.02	15.93	0.94
6LSFM-4BZCY (80-90 μm)	1.14	0.25	0.82	0.52
8LSFM-2BZCY (80-90 μm)	1.13	0.44	0.49	0.36

Table S3: summary of EC cell performance at 500 °C

Cell/interlayer	OCV (V)	Current Density (A cm^{-2}) at 1.5 V	Rp (Ω cm^{-2})	Rs (Ω cm^{-2})
Reference	0.92	0.25	2.03	1.07
No interlayer	0.70	0.06	12.36	4.43
6NiO-4BZCY (<1 µm)	0.96	0.26	2.38	1.07
6NiO-4BZCY (20-30 µm)	0.99	0.40	3.42	0.63
6NiO-4BZCY (60-70 µm)	0.89	0.03	28.42	5.91
6CMF-4BZCY (<1 µm)	0.98	0.15	4.56	2.55
6CMF-4BZCY (20-30 µm)	0.94	0.23	6.17	0.67
6NiO-4LSCF (20-30 µm)	1.00	0.038	57.77	6.7
6LSGM-4BZCY (20-30 µm)	0.98	0.08	19.19	3.66
6LSFM-4BZCY (80-90 µm)	0.92	0.28	1.86	1.08
8LSFM-2BZCY (80-90 µm)	0.97	0.71	1.50	0.46

Supplementary Note 5: Comparing hydrogen production efficiency: To achieve high efficiency of hydrogen production is our original concept for developing DDC. In protonic ceramic cells, low Faradaic efficiency is a major challenge in EC operation, typically in high oxidative atmosphere such as air or oxygen. In our previous works, to achieve reasonable Faradaic efficiency, we used low oxygen content (1% O_2 diluted in inert gas) [11, 13, 14]. However, using inert gas produces more expensive operational cost. In addition, this reaction condition is not applicable for FC operation, which limits the reversibility of cells. It is more promising in air atmosphere (~21% O_2) for air electrode. In our experiment, we used 50% O_2 at the air side to introduce strong oxidation and investigate the improvement of faradaic efficiency of DDC. As we expected, DDC maintained a high Faradaic efficiency (~90%) for 200 h of operation of 500 ^oC.

Many of the reported works showed much high current density in EC operation. However, not many of them discussed the high Faradaic efficiency. Zhen et al. (*Nat. Commun. 2025*) also reported high faradaic efficiency (83~95%) operated in 80% O_2 (see Table S4)[15]. No clear reason for this high and stable Faradaic efficiency was discussed in that work. In addition, Faraday efficiency for long-term operation was not represented in that work. Lui et al. (*Nat. Energy, 2023*) used BSC-PBSCF composited air-electrode [16]. The Faraday efficiency was high (80~90%) operated longer than 250 h. However, they operated the cell with a low oxygen content in air electrode (40%H_2O-60%N_2). Bian et al. (*Nature, 2022*) reports Faradaic efficiency of 70~93% from 70%O_2 in air electrode [17]. No long-term Faradaic efficiency was presented in that report.

In terms of high and stable hydrogen production efficiency, our DDC shows its potential over most of the reported cells in Table S4.

Table S4: Summary of faradaic efficiency of EC operation

Cell	Reaction	Temp. (°C)	Applied Voltage (V)	Faradaic Eff. (%)	Long-term FE	Ref.
Ni-BZCY|BZCY|8LSFM-2BZCY|LSGM|BLC	10%H_2-90%N_2/50%O_2-50%steam	500	1.5 1.4 1.3	73 79 89	>200h	This work
Ni-BZCY|BZCY|6LSFM-4BZCY|LSGM|BLC			1.5 1.4 1.3	95 97 93	N/A	
Ni-BZCY|BZCY|6NiO-4BZCY|LSGM|BLC			1.5 1.4	91 85	N/A	
Ni-BZCYYb|BZCYYb (10μm)|NNAUP-PNC	H_2/20%H_2O-80%O_2	450	1.3~1.5	83~95	N/A	2025 [15]
Fe-Cr|LSM|Ni-BZCY|BZCY-PLD (1 |m)|BGLC-BZCY	N_2-3%H_2O/10% H_2O-air	500	1.5 1.3	N/A	N/A	2024 [18]
Ni-BZCYYb|BZCYYb(3 μm)|BSC-PBSCF	H_2/40%H_2O-60%N_2	400	1.4	80~90	>250	2023 [16]
NiO-BZCYYb|BZCYYb(22 μm)| PNC	H_2/O_2-30% steam	600	1.3~1.5	70~93	N/A	2022 [19]
Ni-BNCYb|BNCYb (10μm)| PBCC	30%H_2-70%Ar/30% steam-Air	600	1.05~1.35	70~95	N/A	2022 [20]
Ni-BHCYb|BHCYb(10μ m)| BCFN	30%H_2-70%Ar/30% steam-Air	600	1.02~1.35	65~95	N/A	2022 [21]
Ni-BZCYYb|BZCYYb (10μm)| PNC	100%H_2-/15%steam-air	500	1.3~1.5	65~70	N/A	2020 [22]

Abbreviation

BGLC : $Ba_{0.5}Gd_{0.8}La_{0.7}Co_2O_{6-\delta}$
BLC : $Ba_{0.6}La_{0.4}CoO_{3-\delta}$
BZCY : $BaZr_{0.44}Ce_{0.36}Y_{0.2}O_{3-\delta}$
BZCYYb : $BaZr_{0.16}Ce_{0.64}Y_{0.1}Yb_{0.1}O_{3-\delta}$
CMF : $Ce_{0.6}Mn_{0.3}Fe_{0.1}O_{2-\delta}$
DDC : Double decker cell
EC : Electrolysis cell
FC : Fuel cell
H^+CP : Proton conducting particles
LSCF : $La_{0.6}Sr_{0.4}Co_{0.2}Fe_{0.8}O_{3-\delta}$
LSFM : $La_{0.6}Sr_{0.4}Fe_{0.8}Mn_{0.2}O_{3-\delta}$
LSGM : $La_{0.9}Sr_{0.1}Ga_{0.8}Mg_{0.2}O_{3-\delta}$
LSM : $(La_{0.8}Sr_{0.2})_{0.95}MnO_{3-\delta}$
LSS : $La_{0.85}Sr_{0.15}ScO_{3-\delta}$
O^{2-}CP : Oxide ion conducting particles
PCFC : Proton-conducting fuel cell
PLD : Pulse layer deposition
SDC : $Sm_{0.2}Ce_{0.8}O_{3-\delta}$
SOFC : Solid oxide fuel cell
SZCY : $SrZr_{0.5}Ce_{0.4}Y_{0.1}O_{3-\delta}$
YSZ : Yttria stabilized zirconia

References

[1] D. Masson, F. Perrozzi, P. Piccardo, M. Viviani, C. Pilot, Z. Stoynov, D. Vladikova, A. Chesnaud, A. Thorel, Shaping of a dual membrane SOFC and first electrochemical tests in a dedicated 3-chamber set-up, ECS Trans. 68 (2015) 1969.

[2] D. Vladikova, Z. Stoynov, A. Chesnaud, A. Thorel, M. Viviani, A. Barbucci, G. Raikova, P. Carpanese, M. Krapchanska, E. Mladenova, Application of yttrium doped barium cerate for improvement of the dual membrane SOFC design, Int. J. Hydrogen Energ. 39 (2014) 21561-21568.

[3] M. Viviani, A.S. Thorel, A. Barbucci, D. Vladikova, A. Chesnaud, I. Genov, G. Raikova, E. Mercadelli, P. Piccardo, M.P. Carpanese, Innovative dual membrane architecture for reversible fuel cells, ECS Tran. 57 (2013) 3143.

[4] A.S. Thorel, J. Abreu, S.A. Ansar, A. Barbucci, T. Brylewski, A. Chesnaud, Z. Ilhan, P. Piccardo, J. Prazuch, S. Presto, K. Przybylski, D. Soysal, Z. Stoynov, M. Viviani, D. Vladikova, Proof of concept for the dual membrane cell: I. Fabrication and electrochemical testing of first prototypes, J. Electrochem. Soc. 160 (2013) F360.

[5] T. Ou, F. Delloro, W.G. Bessler, A.S. Thorel, C. Nicolella, Proof of concept for the dual membrane cell: II. Mathematical modeling of charge transport and reaction in the dual membrane, J. Electrochem. Soc. 160 (2013) F367.

[6] K. Hosoi, T. Sakai, S. Ida, T. Ishihara, $Ce_{0.6}Mn_{0.3}Fe_{0.1}O_{2-\delta}$ as an alternative cathode material for high temperature steam electrolysis using $LaGaO_3$-based oxide electrolyte, Electrochimica Acta 194 (2016) 473-479.

[7] K.-T. Wu, T. Ishihara, Superior syngas product control of $La(Sr)F(Mn)O_3$ perovskite in high-temperature CO_2/H_2O co-electrolysis, Appl. Catal. B-Environ. Energ. 357 (2024) 124335.

[8] Y.S. Chung, T. Kim, T.H. Shin, H. Yoon, S. Park, N.M. Sammes, W.B. Kim, J.S. Chung, In situ preparation of a $La_{1.2}Sr_{0.8}Mn_{0.4}Fe_{0.6}O_4$ Ruddlesden–Popper phase with exsolved Fe nanoparticles as an anode for SOFCs, J. Mater. Chem. A, 5 (2017) 6437-6446.

[9] T. Ishihara, H. Matsuda, Y. Takita, Doped $LaGaO_3$ perovskite type oxide as a new oxide ionic conductor, J. Am.Chem. Soc. 116 (1994) 3801-3803.

[10] A.S. Lesnichyova, S.A. Belyakov, A.Y. Stroeva, A.V. Kuzmin, Proton conductivity and mobility in Sr-doped $LaScO_3$ perovskites, Ceram. Int. 47 (2021) 6105-6113.

[11] K. Leonard, Y. Okuyama, Y. Takamura, Y.-S. Lee, K. Miyazaki, M.E. Ivanova, W.A. Meulenberg, H. Matsumoto, Efficient intermediate-temperature steam electrolysis with Y : $SrZrO_3$–$SrCeO_3$ and Y : $BaZrO_3$–$BaCeO_3$ proton conducting perovskites, J. Mater. Chem. A, 6 (2018) 19113-19124.

[12] B.S. Kang, J. Matsuda, Y.W. Ju, H.H. Kim, T. Ishihara, Nano strain induced double columnar oxide as highly active oxygen-dissociation electrode for Ni-Fe metal supported solid oxide fuel cells, Nano Energ. 56 (2019) 382-390.

[13] K. Leonard, Y. Okuyama, M.E. Ivanova, W.A. Meulenberg, H. Matsumoto, Tailored and improved protonic conductivity through Ba $(ZxCe_{10-x})_{0.08}Y_{0.2}O_{3-\delta}$ ceramics perovskites type oxides for electrochemical devices, ChemElectroChem. 9 (2022) e202101663.

[14] K. Leonard, M.E. Ivanova, A. Weber, W. Deibert, W.A. Meulenberg, T. Ishihara, H. Matsumoto, Anode supported planar 5× 5 cm^2 $SrZr_{0.5}Ce_{0.4}Y_{0.1}O_{2.95}$ based solid oxide protonic fuel cells via sequential tape-casting, Solid State Ion. 379 (2022) 115918.
[15] S. Zheng, W. Wu, Y. Zhang, Z. Zhao, C. Duan, S. Karki, H. Ding, Enhancing surface activity and durability in triple conducting electrode for protonic ceramic electrochemical cells, Nature Commun. 16 (2025) 4146.
[16] F. Liu, H. Deng, D. Diercks, P. Kumar, M.H.A. Jabbar, C. Gumeci, Y. Furuya, N. Dale, T. Oku, M. Usuda, P. Kazempoor, L. Fang, D. Chen, B. Liu, C. Duan, Lowering the operating temperature of protonic ceramic electrochemical cells to <450 °C, Nature Energ. 8 (2023) 1145-1157.
[17] W. Bian, W. Wu, B. Wang, W. Tang, M. Zhou, C. Jin, H. Ding, W. Fan, Y. Dong, J. Li, Revitalizing interface in protonic ceramic cells by acid etch, Nature, 604 (2022) 479-485.
[18] H. Zheng, N. Sata, F. Han, A.M. Dayaghi, F. Iguchi, K. Develos-Bagarinao, T. Norby, M. Stange, R. Costa, Hydrogen production with a protonic ceramic membrane reactor on porous Fe–Cr alloy, ACS Energ. Lett. 9 (2024) 3962-3969.
[19] W. Bian, W. Wu, B. Wang, W. Tang, M. Zhou, C. Jin, H. Ding, W. Fan, Y. Dong, J. Li, D. Ding, Revitalizing interface in protonic ceramic cells by acid etch, Nature, 604 (2022) 479-485.
[20] Z. Luo, Y. Zhou, X. Hu, N. Kane, W. Zhang, T. Li, Y. Ding, Y. Liu, M. Liu, Highly conductive and durable Nb(Ta)-doped proton conductors for reversible solid oxide cells, ACS Energ. Lett. 7 (2022) 2970-2978.
[21] Z. Luo, Y. Zhou, X. Hu, N. Kane, T. Li, W. Zhang, Z. Liu, Y. Ding, Y. Liu, M. Liu, Critical role of acceptor dopants in designing highly stable and compatible proton-conducting electrolytes for reversible solid oxide cells, Energ. Environ. Sci. 15 (2022) 2992-3003.
[22] H. Ding, W. Wu, C. Jiang, Y. Ding, W. Bian, B. Hu, P. Singh, C.J. Orme, L. Wang, Y. Zhang, D. Ding, Self-sustainable protonic ceramic electrochemical cells using a triple conducting electrode for hydrogen and power production, Nature Commun. 11 (2020) 1907.